Response of a silicon photodiode to pulsed radiation

Robert E. Vest and Steven Grantham

Both the integrated-charge and the peak-voltage responsivity of a 1-cm^2 Si photodiode optimized for the extreme ultraviolet have been measured with 532-nm-wavelength pulsed radiation. The peak power of the optical pulse is varied from 35 mW to 24 kW with a pulse width of 8.25 ns. A decrease in responsivity is observed with increasing pulse energy, and a model is presented that accounts for the observed loss of responsivity. The integrated-charge responsivity decreases because the presence of photogenerated majority carriers increases the direct recombination rate. The peak-voltage responsivity is reduced because the electric susceptibility of the electrons and holes in the depletion region increases the capacitance of the device. The influence of an applied reverse bias on both responsivities is investigated. The integrated-charge responsivity is found to be identical, with a 1% uncertainty, to the cw responsivity of the device if the energy dependence is considered.

OCIS codes: 120.5630, 120.3940, 230.5170.

1. Introduction

The advent of extreme-ultraviolet lithography (EUVL) based on 13.4-nm wavelength radiation will introduce new requirements on the radiometry of pulsed sources in the EUV. All the candidate sources for EUVL produce pulses of radiation with pulse lengths from ~10 ns to several hundred nanoseconds. These sources must deliver ~150 W of average power to the intermediate focus of the EUVL stepper,[1] which implies an average power of ~5 W at the wafer plane. If a source operates at 10 kHz, this represents a peak power of 2.5 kW for a discharge source (~200 ns pulse) or of 50 kW for a laser-produced plasma (~10-ns pulse). If the target repetition rate is not achieved, the peak power must be greater to reach the target average power.

The rapid generation of a large number of charge carriers followed by a significant dark period will not necessarily produce the same response in a photodiode as will a continuous-wave (cw) input of the same average power. Calibration facilities in the EUV are typically based on synchrotron radiation from an electron storage ring,[2–6] which is effectively a cw source for all but the fastest photodiodes. Fast devices typically have small active areas and are not favored as transfer standard detectors. Because relatively large area (as much as 100-mm^2) photodiodes are likely to be used to transfer a calibration from a synchrotron-radiation-based system to the pulsed EUVL application, it is important to identify and understand the differences between the photodiode's responses to pulsed and cw illumination and to understand the saturation mechanisms at high peak powers.

Stuik and Bijkerk have investigated[7] the linearity of Si photodiodes at pulse lengths from 170 ns to 1.2 ms for a few peak power levels from 3.5 to 118 mW. They report that the charge collected by an oscilloscope is linearly proportional to the pulse energy and that, without application of a reverse-bias voltage to the photodiode, the peak current, and therefore peak voltage, is equivalent, within ±2%, to the cw value for pulse lengths longer than 3 μs. They report a significant decrease in peak current at shorter pulse lengths and attribute this roll-off to the impulse response of the photodiode. The application of 9-V reverse bias reduces the minimum pulse length for equivalent responsivity to approximately 500 ns. Stuik and Bijkerk generated pulsed radiation from a cw laser and a rotating mirror, a design that limits the peak power of the pulse to the cw laser power. The mirror's rotation rate determines the pulse length, and hence the pulse energy, for a given laser power. The illumination frequency is also a function of pulse length.

Seely *et al*. have reported[6] on the time responses of Si photodiodes and have compared several important

The authors are with the National Institute of Standards and Technology, 100 Bureau Drive, Gaithersburg, Maryland 20899-8411. R. E. Vest's e-mail address is rvest@nist.gov.

Received 28 February 2003; revised manuscript received 22 May 2003.

0003-6935/03/255054-10$15.00/0

parameters at EUV wavelengths with the same parameter at a wavelength of 670 nm. They report that the rise time of a photodiode is governed primarily by the input pulse width and the bandpass of the electronics used for measurement. The fall time is determined primarily by the photodiode capacitance. They investigated the capacitance as a function of reverse bias and wavelength and found no significant difference in capacitance when the sample photodiode was illuminated by 600-ps pulses of EUV radiation from a synchrotron (4–16-nm wavelength) and a 68-ps pulse from a diode laser operating at 670-nm wavelength. One important implication of this result is that the electrical behavior of the photodiode and the photogenerated charges is independent of the mechanism by which the electrons are excited into the conduction band. At EUV wavelengths the photon is absorbed by a direct bandgap transition, and the primary electron quickly thermalizes, generating secondary electrons. At visible wavelengths the photon is absorbed by an indirect bandgap transition, and there is no gain in electron number. The time structure and electrical properties of the photodiode response are independent of which mechanism (indirect bandgap excitation or direct bandgap excitation with electron multiplication) generates the electron–hole pairs. The implications of this result for the use of 532-nm-wavelength radiation as a proxy for 13.4-nm radiation—the experimental approach adopted by Stuik and Bijkerk and by us—are discussed below. Seely *et al*. report observations similar to those reported here—capacitance decreases with reverse bias and increases because of the presence of carriers in the depletion region, peak voltage varies inversely with capacitance, and collected charge is independent of reverse bias—but focus their analysis on the time structure of the photodiode's output pulse.

We extend the investigation of photodiode response to pulsed illumination by using a frequency-doubled, *Q*-switched Nd:YAG laser (532-nm wavelength) as a pulsed source to determine the responsivity of the photodiode as a function of incident pulse energy. The optical pulse has an approximately Gaussian time structure, with a full width at half-maximum of 8.25 ns. The pulse length is much less than can be achieved by a mechanical modulation of a cw beam and matches that of many candidate EUVL sources. The pulse energy and illumination frequency are independent of the pulse length, but the pulse length is fixed. The use of a *Q*-switched laser allows us to reach peak power regions that are inaccessible by a modulated cw laser system. We report here results for 35-mW to 25-kW peak power.

Throughout this paper we use the term "responsivity" to refer to both the peak voltage developed per unit pulse energy (typically stated in volts per joule) and the total charge generated per unit pulse energy (typically stated in charge coulombs per joule). The integrated-charge responsivity is closely related to the responsivity in the cw regime, in which the term means photocurrent generated per unit incident power (typically stated in amperes per watt). The use of this term for the voltage signal is a straightforward generalization from the familiar meaning in the cw regime.

2. Experimental Design

In the investigation reported here, the 532-nm emission from a frequency-doubled Nd:YAG laser is used as a proxy for EUV radiation at 13.4-nm wavelength. The penetration depth of the incident radiation differs by ~35% at these two wavelengths (0.59 μm at 13.4-nm wavelength and 0.82 μm at 532-nm wavelength).[7–10] The intensity of the electromagnetic wave propagating in the Si is an exponential function of depth, with a decay rate that is inversely proportional to the penetration depth. The difference between the relative intensity (intensity normalized to the intensity at the surface) at 532 nm and that at 13.4 nm is maximum at a depth of ~0.68 μm, where the intensity at 532 nm is ~28% greater. The initial spatial distribution of photogenerated charge carriers is determined by the local intensity of the radiation as it propagates in the Si. The observation of Seely *et al*.[6] that the electrical response is independent of the excitation mechanism indicates that the evolution of the charge carrier distribution in the Si, and hence the response of the photodiode, is not dependent on the details of the absorption mechanism. The electrical response generated by radiation of 532-nm wavelength will evolve in a similar manner to that generated by radiation of 13.4-nm wavelength because the initial charge carrier distribution will be similar. Thus the energy dependence of the responsivity should be qualitatively similar in the two cases. Further investigation of the similarity between 532- and 13.4-nm wavelength radiation is under way at the National Institute of Standards and Technology (NIST) to quantify the effects of the different absorption mechanisms (direct and indirect bandgap), of the difference in penetration depth, and of the different absorption characteristics in the oxide layer.

The sample detector is a commercially available Si photodiode with 1-cm^2 active area optimized for use in the far-UV and EUV spectral regions. The passivating SiO_2 layer is thin, ~9 nm, to permit transmission into the Si over a broad spectral range, from x ray to IR. Furthermore, the SiO_2 layer was grown by a rapid thermal process that incorporates N into the Si–SiO_2 interface to increase the radiation hardness of the device.[11] The photodiode's internal structure is n-on-p, and the device is illuminated from the front side.

The passivating oxide layer introduces a difference between the absorption characteristics of the photodiode at 532- and 13.4-nm wavelengths. That is, the oxide is transparent at 532-nm wavelength but absorbs approximately 8% of the incident radiation at 13.4-nm wavelength. Absorption in the oxide layer does contribute to the measured photocurrent in cw applications[12–14] and will most likely contribute charge carriers in pulsed applications as well. The charge carrier collection efficiency from the oxide has

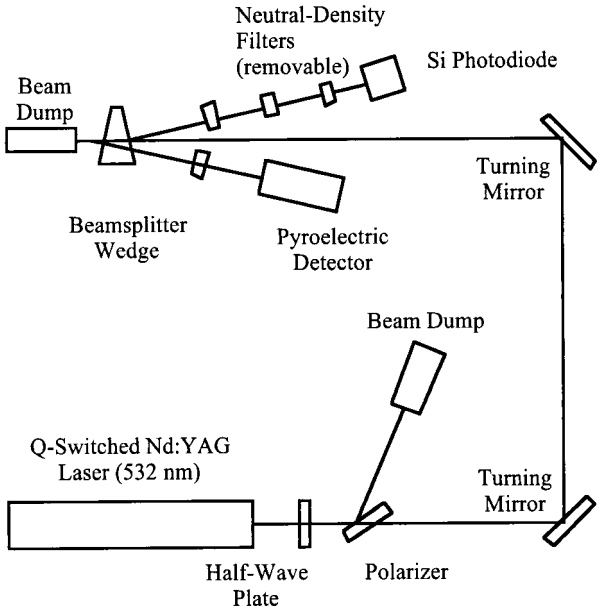

Fig. 1. Schematic diagram of the optical system. The half-wave plate and the polarizer form a variable attenuator that maintains a constant pulse energy on the pyroelectric detector. One controls the pulse energy incident upon the Si photodiode by removing and inserting combinations of neutral-density filters.

been estimated to be 15%, and the carrier collection efficiency in Si is near 100%.[6,15] The charge contributed to the photodiode response by absorption in the oxide layer is approximately 1.3% of the charge generated in the Si.

The responsivity of the Si photodiode is measured by comparison with a pyroelectric detector calibrated by the NIST Optoelectronics Division.[16] A pulse from the *Q*-switched laser is split into two measurement beams by a glass wedge. One beam is detected by the pyroelectric detector, and the other is sent to the sample Si photodiode. The beam incident upon the beam splitter and upon both detectors has a diameter of 5 mm. In the photodiode arm, a number of calibrated neutral-density filters can be inserted to vary the pulse energy incident upon the photodiode by 6 orders of magnitude. A variable attenuator located upstream of the wedge is used to maintain the pulse energy incident upon the pyroelectric detector within 5% of its calibration energy of 200 μJ. A schematic diagram of the optical system is shown in Fig. 1.

The linearity of the pyroelectric detector over a large dynamic range is suspect,[17] and, because we seek to determine the photodiode's behavior under pulsed conditions, we cannot assume that the Si photodiode will be linear under pulsed illumination. Therefore the characterization of the optical system's components was carried out with a cw laser. Typical Si photodiodes of the same type as and similar size to the sample are known to have a linear response up to 3 mA of photocurrent (approximately 10 mW at 532 nm) for cw illumination.[18] A frequency-doubled, diode-pumped Nd:YAG laser with a nominal output power of 1 mW was used as a cw source. The transmission of the neutral-density filters was measured *in situ* by an insertion technique, and thermal and positional effects were identified and controlled. Effects that were due to multiple reflections propagating unattenuated between filters in a series were quantified, and an appropriate correction was applied. The relative combined standard uncertainty of the transmission of a series of filters ranges from 0.1% to 1%, depending on which filters are in the optical path. (Throughout this paper, all stated uncertainties are the combined standard uncertainty of the quantity; i.e., the coverage factor is $k = 1$.) An additional neutral-density filter (nominal optical density, 1.0) is permanently located in each beam reflected from the glass wedge. The beam-splitter ratio of the system of the wedge and two permanent filters was measured with a relative combined standard uncertainty of less than 0.1% by use of the cw laser in a cross-calibration technique that does not require knowledge of the detector efficiencies.

After the optical system was characterized, the output pulse from each detector (pyroelectric reference and Si photodiode sample) for a single shot from the *Q*-switched laser was measured by two different oscilloscopes. The pyroelectric detector's output was measured with a 100-MHz (1-Gsample/s) digital oscilloscope; the photodiode output was measured with a 500-MHz (1-Gsample/s) digital oscilloscope with an input impedance of 50 Ω. Each trace was transferred to the control computer, in which the pulse was analyzed. The laser pulse energy was determined from the peak voltage of the pyroelectric detector output. The photodiode signal was measured both as the peak voltage and as the total charge, determined by numerical integration of the voltage trace from the oscilloscope:

$$Q = \int_{\text{pulse}} I(t)\mathrm{d}t = (1/R) \int_{\text{pulse}} V(t)\mathrm{d}t, \qquad (1)$$

where Q is the total charge, $I(t)$ is the instantaneous current, $V(t)$ is the instantaneous voltage recorded by the oscilloscope, and R is the load resistance of the oscilloscope's input electronics and the bias tee (see below for a discussion of the bias electronics). The photodiode's responsivities in total charge per unit energy and peak voltage per unit energy were recorded simultaneously in a computer file. The measurements were repeated at a single incident energy until the statistical component of the relative combined standard uncertainty was less than 2%. In no case were more than 25 measurements taken, nor fewer than 5 measurements.

The Si photodiode was connected to the oscilloscope through a bias tee, a schematic diagram of which is shown in Fig. 2. Two variations on the bias tee were used. In the first configuration, called the low-Z tee, the value of the resistor, R_1, was 1 kΩ; in the second configuration, called the high-Z tee, R_1 was 100 kΩ. Because of the ac Fourier components, a pulse sees the capacitors to ground (in the dashed box in Fig. 2)

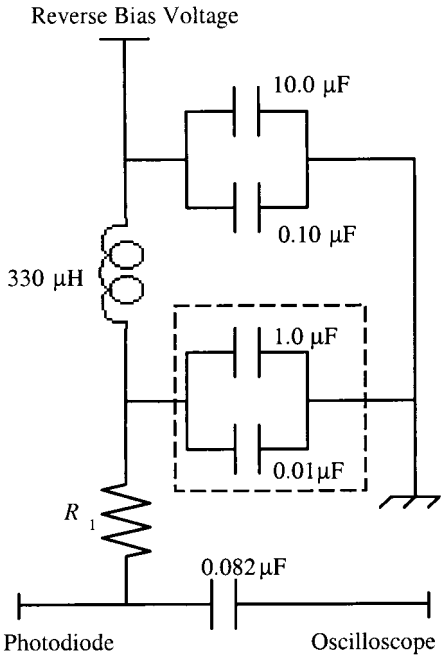

Fig. 2. Schematic diagram of the bias tee. The resistor R_1 was originally 1 kΩ (low-Z tee) but was replaced with 100 kΩ (high-Z tee). For high-frequency components such as the Fourier components of a fast pulse, the capacitors in the dashed box are a low-impedance path to ground. The photodiode output pulse sees the resistance R_1 in parallel with the oscilloscope's input impedance.

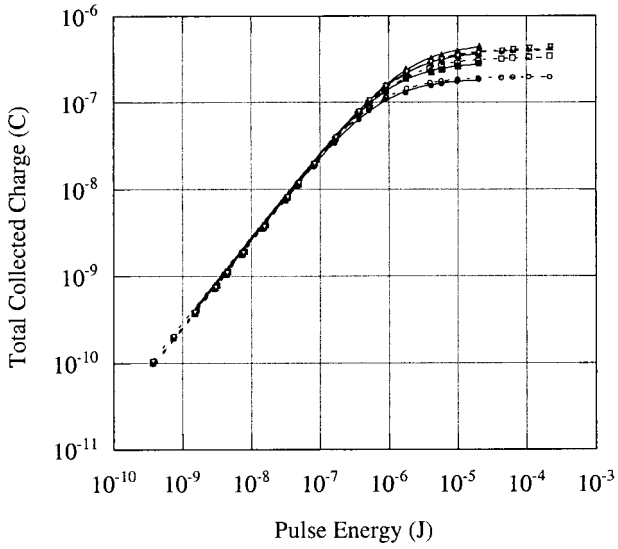

Fig. 3. Total charge collected by an external circuit as a function of incident pulse energy. The points are data with reverse-bias values of 2 V (circles), 4 V (squares), 6 V (diamonds), 8 V (triangles), and 10 V (inverted triangles). Filled symbols with solid-curve fits were obtained with the low-Z bias tee; open symbols with dashed-curve fits were obtained with the high-Z bias tee. The curves are the expected signal based on the curve fits to the responsivity data shown in Fig. 4. At sufficiently low pulse energy, the signal is not a function of reverse bias. The onset of significant saturation is a function of reverse bias.

as a low impedance, and the load resistance is the oscilloscope's input impedance in parallel with R_1 from the bias tee. In the low-Z tee, the resistance seen by the photodiode is 47.6 Ω, a 5% difference from the 50-Ω input impedance of the oscilloscope. This reduced value of resistance must be substituted for R in Eq. (1). For the high-Z tee the difference is less than 0.05%, and the influence of the bias tee may be neglected. A fast-Fourier-transform analysis of the output pulse shows that it is composed of frequency components up to 500 kHz, easily within the bandpass of the oscilloscope. There is no significant power contained in the low-frequency band, where the capacitor series impedance is significant compared to R_1.

3. Results

The total charge collected is shown in Fig. 3 as a function of pulse energy E_p. The integrated-charge responsivity $\eta_Q(E_p)$ is shown in Fig. 4. The responsivity at a given pulse energy is reproducible within 1% for all measured reverse-bias conditions in the 0.3-nJ (peak power, 35 mW) to 50-nJ (6 W) range. A slow trend of decreasing responsivity with increasing pulse energy is observed in this energy range. At higher pulse energies, the device is clearly in saturation. The data of Fig. 4 have been fitted to an expression of the form

$$\eta_Q(E_p) = \frac{1}{\alpha_Q + \beta_Q E_p}, \tag{2}$$

where α_Q and β_Q are fit parameters, which predicts the observed slope, even at low pulse energies. This dependence on energy arises from the dependence of the

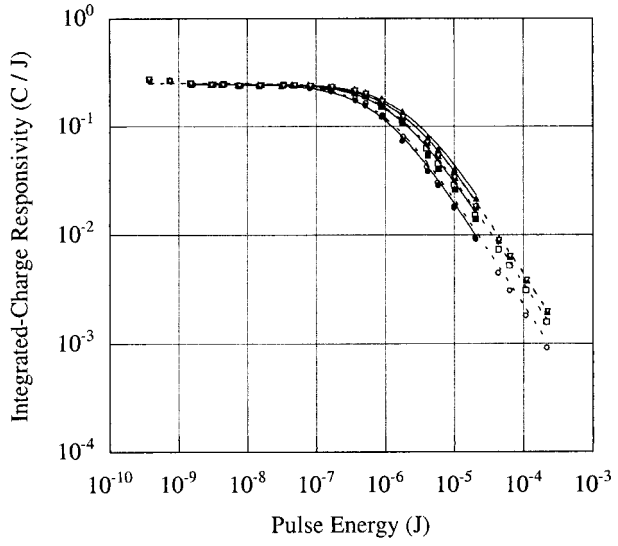

Fig. 4. Integrated-charge responsivity as a function of incident pulse energy. The points are data with reverse-bias values of 2 V (circles), 4 V (squares), 6 V (diamonds), 8 V (triangles), and 10 V (inverted triangles). Filled symbols with solid-curve fits were obtained with the low-Z bias tee; open symbols with dashed-curve fits were obtained with the high-Z bias tee. The curves are the curve fitting results of the data to Eq. (2).

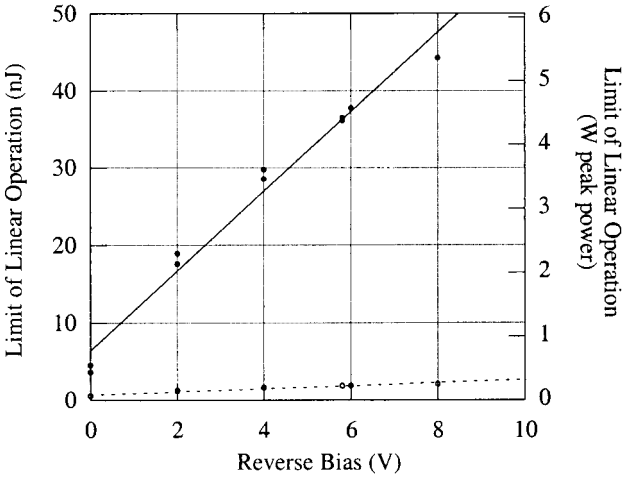

Fig. 5. Maximum pulse energy that produces a linear response in the Si photodiode as a function of reverse-bias voltage when the integrated charge (filled circles) and peak voltage (open circles) are measured. Here the limit is taken as the pulse energy at which the responsivity is reduced by 2% from the value in the low-power limit.

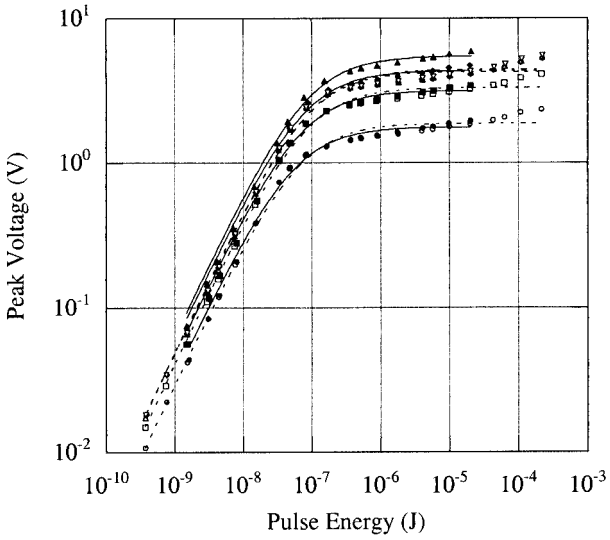

Fig. 6. Peak voltage detected by an external circuit as a function of incident pulse energy. The points are data with reverse-bias values of 2 V (circles), 4 V (squares), 6 V (diamonds), 8 V (triangles), and 10 V (inverted triangles). Filled symbols with solid-curve fits were obtained with the low-Z bias tee; open symbols with dashed-curve fits were obtained with the high-Z bias tee. The curves are the expected signal based on the curve fits to the responsivity data shown in Fig. 7. The signal is a function of reverse bias at all the pulse energies studied.

direct recombination rate on the concentration of photogenerated carriers and is discussed more fully below.

The pulse energy at which saturation becomes significant is increased by the reverse-bias voltage, as shown in Fig. 5. Typically, the application requirements and measurement system's precision will determine the appropriate limit of linearity for a particular application. We have chosen a limit at which the responsivity is reduced by 2%, or twice the measurement reproducibility, from the low-power limit. Figure 5 also shows the limit of linear operation for the peak-voltage signal, which has a smaller dynamic range than the integrated-charge signal.

Charge Q generated per unit of energy incident upon the device is a characteristic property of the photodiode, determined by the internal quantum efficiency and reflectivity of the device. In pulsed applications, the charge initially generated is given by $Q = \eta_Q(0)E_p$, even if some charge is later lost without being detected. In a cw application the rate of charge generation is proportional to the incident power, and the cw responsivity should be equivalent to the integrated-charge responsivity for pulsed radiation. Extrapolation of the nine independent curve fits from Fig. 4 to a low-power regime ($E_p \approx 0$) produces a common value of $\eta_Q(0) = (0.2493 \pm 0.0026)$ C/J. The reproducibility of the intercept implies a statistical uncertainty component of 0.3%, which is much less than the 1% calibration uncertainty of the pyroelectric detector. The sample photodiode was calibrated at the NIST SIRCUS facility[19] by NIST's Optical Technology Division.[20] SIRCUS is a detector calibration facility based on cw lasers and the High Accuracy Cryogenic Radiometer.[21] The cw calibration, based on a calibrated trap detector in radiant power mode, was performed at a power level of 12 μW (in the low-power regime, compared to the lower-limit peak power of 35 mW in the current experiment) and yielded a responsivity of (0.2489 ± 0.0012) A/W. (The unit change from amperes per watt to coulombs per joule leaves the numeric value of responsivity unchanged.) The difference between the pulsed-radiation, integrated-charge responsivity and the cw responsivity of the photodiode is (-0.0004 ± 0.0029) C/J, or $0.2\% \pm 1.1\%$. The equivalence of pulsed and cw responsivity is confirmed, but the comparison must take the dependence of the pulsed responsivity on pulse energy into account.

Figure 6 shows the peak voltage developed by the photodiode as a function of incident pulse energy. The signal developed is a function of reverse-bias voltage. This dependence on bias arises from the increase in the width of the depletion region, and hence the decrease in junction capacitance, that accompanies the application of reverse bias. The peak-voltage responsivity is shown in Fig. 7 and has been fitted to an expression of the form of Eq. (2). The dependence of the peak-voltage responsivity on pulse energy arises from the electric susceptibility of the electron–hole system in the depletion region and is discussed more fully below.

4. Discussion

Figure 8 is a schematic diagram of a photodiode, illustrating the depletion region that forms at the junction. The majority carriers from each side of the boundary diffuse across the junction and recombine, leaving a region depleted of free carriers but with ionized dopants. The charges trapped at the dopant sites generate an electric field oriented from the

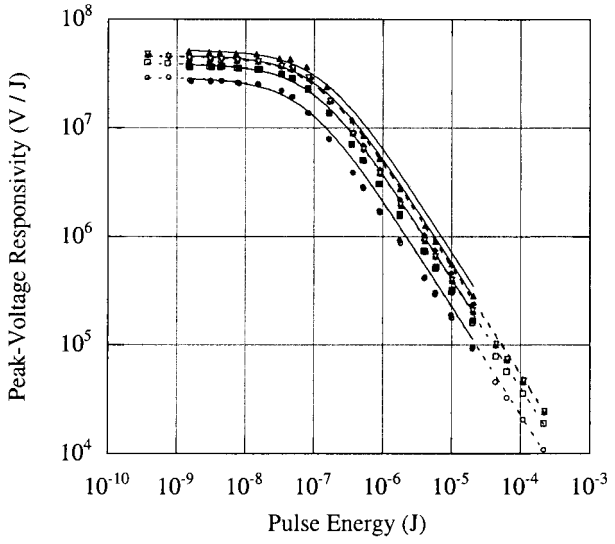

Fig. 7. Peak-voltage responsivity as a function of incident pulse energy. The points are data with reverse-bias values of 2 V (circles), 4 V (squares), 6 V (diamonds), 8 V (triangles), and 10 V (inverted triangles). Filled symbols with solid-curve fits were obtained with the low-Z bias tee; open symbols with dashed-curve fits were obtained with the high-Z bias tee. The curves are the curve fitting results of the data to Eq. (2).

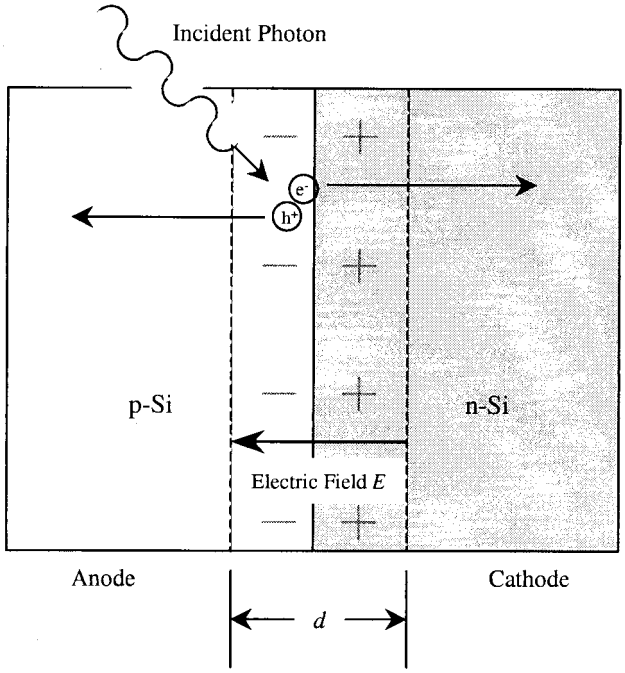

Fig. 8. Schematic diagram of a photodiode. At the junction between the p-type and the n-type Si regions the free carriers from each side diffuse across the boundary and recombine, leaving a depletion region of width d with no free carriers and ionized dopants. The ionized dopants generate an electric field across the depletion region, oriented from the n-type to the p-type Si. An incident photon generates an electron–hole pair that is separated by the field: the holes drift to the anode, and the electrons drift to the cathode. The depletion region is modeled as a capacitive electrical element in the photodiode circuit.

n-type Si to the p-type Si. An incident photon generates one or more electron–hole pairs if the photon carries sufficient energy. The electric field causes the holes to drift toward the anode and the electrons to drift toward the cathode. The application of reverse bias to the photodiode increases the internal field at the junction and increases the width of the depletion region.

We model the photodiode as a parallel-plate capacitor, with the depletion region of the p–n junction as the capacitive element. The photodiode capacitor is charged by photogenerated electron–hole pairs when a pulse of radiation is incident upon the device. As the excited pairs are separated by the internal electric field, a potential difference $V = Q/C$ develops between the photodiode's anode and cathode. The capacitor is then discharged through an external circuit, forming a simple RC network. An oscilloscope measures the potential across the discharge network as a function of time, and the total charge on the capacitor is proportional to the integral of this voltage, as shown in Eq. (1). The capacitance C of the photodiode is determined by active area A, width d of the depletion region, and permittivity ε of the material in the depletion region:

$$C = \varepsilon A/d. \tag{3}$$

The width of the depletion region is a function of the applied reverse bias V and is given by[22]

$$d = k(\phi + V)^{p}, \tag{4}$$

where k is a constant whose value is determined by material properties (dielectric constant, dopant concentration, etc.), ϕ is the internal barrier potential of the p–n junction, and p is determined by the doping profile across the depletion region. The value of the exponent p is 1/2 for uniform doping (the abrupt junction model) and 1/3 for dopant concentrations that are linear with depth.[23]

We define a geometric fill factor γ for the illumination such that energy E_p contained in the pulse is deposited in area γA, where A is the active area of the photodiode. The mean energy density is then $E_p/\gamma A$.

A. Integrated Charge

The integrated-charge responsivity $\eta_Q(E_p)$ of the photodiode has a dependence on pulse energy E_p because the increased concentration of majority carriers decreases the recombination time at high incident pulse energies. For typical values[22] of the carrier mobility ($\sim 10^{-1}$ m^2 V^{-1} s^{-1}), depletion region width ($\sim 10^{-6}$ m), and junction potential ($\sim$1 V), the time required for the carriers to cross the depletion region at their scattering-limited drift velocity is found to be of the order of 10^{-11} s. Recombination processes are much slower,[22] and we assume that all significant recombination takes place with thermally generated minority carriers after the charges are separated. The positive voltage pulse is taken from the anode of the photodiode, and the signal is generated by holes, the

majority carrier. The local direct recombination rate in a small volume element dV at the anode is proportional to the number of majority carriers in the volume element. In terms of carrier concentrations, the local recombination rate is given by

$$\frac{1}{\tau_n} = M\left(\frac{p_0}{dV} + \frac{n_c}{dV}\right)dV, \tag{5}$$

where τ_n is the minority carrier lifetime, p_0 is the number of majority carriers in the volume element dV at thermal equilibrium, and M is a material property of the semiconductor that may depend on dopant concentrations. The quantity n_c is the number of carriers generated in dV:

$$n_c = \frac{\eta_Q(0)}{q}\frac{E_p}{\gamma A z}\,dV, \tag{6}$$

where q is the electronic charge and z is the effective depth of the region containing the carriers. Note that z is not the width of the depletion region but rather the length of a column of charge carriers extending from the edge of the depletion region into the undepleted Si. The photogenerated charge is discharged through the load resistance in some finite time, and some charge is lost to recombination during the discharge process. When the recombination time is comparable to the discharge time, a significant fraction of the photogenerated charge may be lost to direct recombination without being measured by the external circuit. The fraction of charge f_Q that is collected from volume element dV is proportional to the local recombination time:

$$f_Q = l\tau_n = \frac{l}{Mp_0 + [M\eta_Q(0)/q\gamma A z]E_p dV}, \tag{7}$$

where l is a constant. In the low-energy regime ($E_p \approx 0$), all the charge is collected and f_Q must be unity, implying that $l = Mp_0$. The responsivity $\eta_Q(E_p)$ is then

$$\eta_Q(E_p) = \eta_Q(0)\frac{1}{1 + [\eta_Q(0)/qp\gamma A z]E_p} = \frac{1}{\alpha_Q + \beta_Q E_p}, \tag{8}$$

where $p = p_0/dV$ is the majority carrier concentration at thermal equilibrium. Equation (8) has the form of Eq. (2). An analogous argument leads to the same result for the negative pulse generated at the cathode by electrons but with the majority and minority roles of the holes and electrons reversed.

Figure 9 shows the empirically determined dependence of the parameters α_Q and β_Q on the reverse-bias voltage. The parameter $\alpha_Q = 1/\eta_Q(0)$ is independent of reverse bias. The parameter β_Q varies inversely as the square of the depletion region width and is fitted by an expression of the form

$$\beta_Q = \frac{1}{m(0.64 + V)^{2p}}, \tag{9}$$

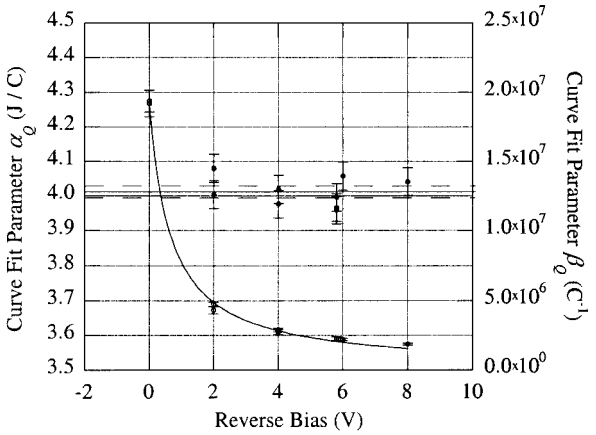

Fig. 9. Integrated-charge responsivity curve fitting parameters as a function of reverse bias. The parameters plotted here are from the curve fits to the data in Fig. 4. The parameter α_Q (filled circles) is independent of reverse bias. The solid horizontal line is the mean value, and the dashed lines indicate the uncertainty of the mean. The parameter β_Q (open circles) is fitted to Eq. (9) and varies as $(\phi + V)^{-1}$, where $\phi = 0.64$ V is the barrier potential of the junction and V is the reverse bias.

where m is a constant, 0.64 V is the internal barrier potential of the p–n junction (the value is derived from the peak–voltage results discussed below), and p is the doping-profile-dependent parameter from Eq. (4). The fitted value of p is 0.49 ± 0.01, showing that β_Q varies inversely as the junction potential. This dependence on junction potential may arise from the dependence of the depletion region's width (and hence the junction's capacitance and device speed), the thermal equilibrium carrier concentration on the junction potential, or the charge carrier's kinetic energy during the transit of the depletion region.

B. Peak Voltage

The peak voltage of the photodiode signal occurs early in the output pulse and does not depend on the recombination rate as long as the device's rise time is short compared to the recombination time. Peak-voltage responsivity $\eta_v(E_p)$ is given by

$$\eta_v(E_p) = \eta_Q(0)/C, \tag{10}$$

and the dependence on pulse energy E_p arises from changes in capacitance C when photogenerated carriers are present in the depletion region.

Each photogenerated electron–hole pair in the depletion region contributes a dipole moment $\Delta p_c = \xi_c E$ in the presence of the internal electric field E. The electric polarization (dipole moment per unit volume) of the electron–hole system is $P_c = n_c \Delta p_c/\gamma A d$, and the total polarization of the depletion region, including contributions P_l from the lattice atoms, is

$$P = P_l + P_c = (\chi_l + \chi_c)E = \left(\chi_l + \frac{n_c \xi_c}{\gamma A d}\right)E, \tag{11}$$

where χ are the electric susceptibilities of the lattice elements and carriers, $n_c = E_p \eta_Q(0)/q$ is the total

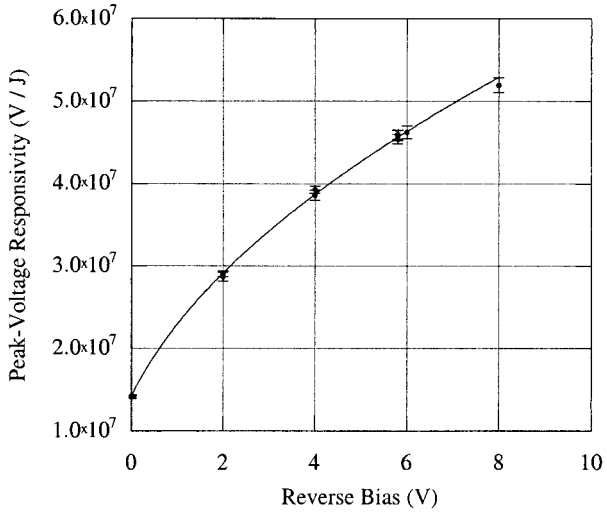

Fig. 10. Peak-voltage responsivity extrapolated to zero pulse energy to show the intrinsic dependence of the junction capacitance on reverse bias. The curve is a curve fit of the data to Eq. (13).

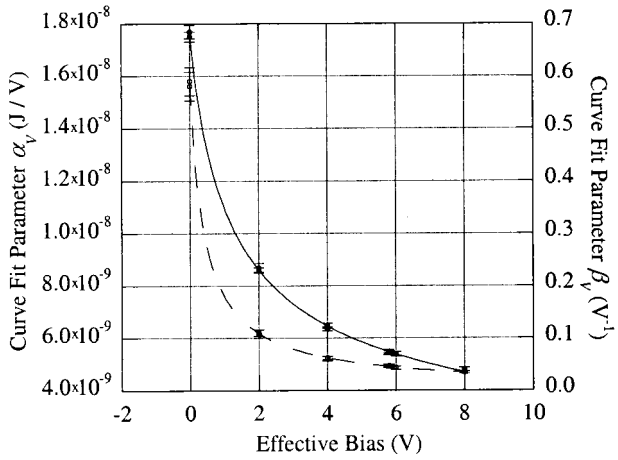

Fig. 11. Peak-voltage responsivity curve fitting parameters as a function of reverse bias. The parameters plotted here are from the curve fits to the data in Fig. 7. The parameter α_v (filled circles) is fitted to Eq. (14) and varies as $(\phi + V)^{-0.5}$, whereas the parameter β_v (open circles) is fitted to Eq. (15) and varies as $(\phi + V)^{-1}$, where ϕ is the barrier potential of the junction and V is the reverse bias.

number of carriers generated, and γAd is the volume of the illuminated portion of the depletion region. The permittivity ε of a material is the sum of the permittivity of free space ε_0 and the susceptibility of the material. Combining Eqs. (10) and (3) with Eq. (11) then yields the peak-voltage responsivity of the device:

$$\eta_v(E_p) = \frac{\eta_Q(0)}{\frac{A}{d}(\varepsilon_0 + \chi_l) + [\xi_c \eta_Q(0)/\gamma q d^2]E_p} = \frac{\eta_Q(0)}{\alpha_v + \beta_v E_p}, \tag{12}$$

which has the form of Eq. (2). The value of $\eta_Q(0)$ used in the curve fits is 0.2493 C/J, taken from the integrated charge results above.

The device's responsivity without the influence of photogenerated carriers is determined from the low-power ($E_p \approx 0$) extrapolation of the curve fitting results. Figure 10 shows the low-power responsivity as a function of reverse bias. The data are fitted to an expression of the form

$$\eta_v(0) = \frac{\eta_Q(0)d}{A\varepsilon} = n(\phi + V)^p, \tag{13}$$

where n is a constant, ϕ is the interior barrier potential, and the exponent p is a function of the doping profile. The fitted value of ϕ is (0.62 ± 0.06) V and that of p is 0.50 ± 0.02, which indicates that the doping concentration is uniform in the depletion region and that the abrupt-junction model is valid for this device.[22,23]

The fit parameters from Eq. (12) are both expected to be a function of reverse bias. The first parameter, α_v, varies as $1/d$, and the second parameter, β_v, varies as $1/d^2$. Figure 11 shows the fit parameters as a function of reverse bias and fits of the data to the explicit expressions in terms of the depletion width d:

$$\alpha_v = \frac{x}{d} = \frac{1}{s(\phi + V)^p}, \tag{14}$$

$$\beta_v = \frac{y}{d^2} = \frac{1}{t(\phi + V)^{2p}}, \tag{15}$$

where s and t are constants. The fit parameters for α_v are ϕ = (0.66 ± 0.05) V and p = 0.51 ± 0.02, confirming the expected behavior of α_v and reproducing the doping profile and the barrier potential values from the $\eta_v(0)$ fit parameters. The fit parameters for β_v are ϕ = (0.38 ± 0.04) V and p = 0.46 ± 0.02. The results for β_v are slightly different from the expected dependence, perhaps because the electron–hole system is not a linear dielectric material or because the polarization P_c varies significantly over the width of the depletion region.

The best estimate of the interior barrier potential is taken to be the weighted average of the $\eta_v(0)$ and α_v

Table 1. Photodiode Parameters Determined from Curve Fits to Responsivity Data

Fitted Quantity[a]	Barrier Potential ϕ(V)[b]	Doping Parameter, p
β_Q	–	0.49 ± 0.01
α_v	0.66 ± 0.05	0.51 ± 0.02
β_v	0.38 ± 0.04	0.46 ± 0.02
$\eta_v(0)$	0.62 ± 0.06	0.50 ± 0.02

[a] α_Q = (4.011 ± 0.014) J/C implies that the intrinsic responsivity is $\eta_Q(0)$ = (0.2493 ± 0.0009) C/J, where the uncertainties reflect only the statistical component of the total uncertainty.

[b] The best estimate of ϕ = (0.64 ± 0.04) V is obtained as the weighted average of the α_v and $\eta_v(0)$ results.

curve fitting results, yielding $\phi = (0.64 \pm 0.04)$ V. This is the value that was a fixed input to the curve fit of β_Q as a function of V in the integrated charge discussion above. The values of the photodiode parameters obtained from the curve fits are summarized in Table 1.

5. Conclusions

A model has been developed that describes both the integrated-charge and the peak-voltage responsivities of a Si photodiode with pulsed incident radiation. The integrated-charge signal saturates because of the loss of photogenerated carriers to direct recombination at the photodiode cathode or anode. This loss mechanism is an ever-present phenomenon rather than a threshold phenomenon. The magnitude of the saturation effect is negligible at sufficiently low pulse energies and becomes more significant as the pulse energy increases. The low-power limit of the integrated-charge responsivity has been shown to agree with a low-power cw measurement of photodiode responsivity with a relative combined standard uncertainty of 1%.

We have shown that the peak-voltage responsivity can be modeled as depending on pulse energy through a polarization mechanism, with the electrons and holes acting as a polarizable dielectric medium in the depletion region. Because the peak voltage occurs early in the pulse, it is not affected by the recombination rate as long as the device's rise time is short compared to the minority carrier lifetime. Although the peak-voltage responsivity is not constant, it does not saturate, in that the signal arises from all the generated charge without regard to subsequent recombination losses.

One implication of the photodiode's nonlinear response to pulsed radiation is that the sensitivity is not constant. The sensitivity is defined[24] as the change in the response divided by the corresponding change in the pulse energy and is calculated as the derivative of response with respect to energy. The photodiode becomes less sensitive with increasing pulse energy. Because of this decreasing sensitivity, the relative uncertainty of an energy measurement increases with pulse energy. For example, if the photodiode in this study were reverse biased at 2 V and the charge were measured with a relative uncertainty of 1%, the relative uncertainty of the energy would be near 1% for pulse energies below 240 nJ. The relative uncertainty is doubled to 2% at a pulse energy of 365 nJ and reaches 5% at 1 μJ. The responsivity at these three energies is reduced by 25%, 30%, and 55%, respectively, from the low-power limit $\eta_Q(0)$. Although it is possible to use the detector in the saturated regime with reasonably low uncertainty by taking account of the nonlinear responsivity, the uncertainty grows dramatically at pulse energies for which the responsivity is less than half of the low-power limit.

As discussed above, EUV lithography will likely require the average power at the wafer plane to be ~5 W at 10 kHz, and the pulse energy will be of the order of 500 μJ. At this pulse energy the integrated-charge responsivity with 2-V reverse bias is reduced to ~0.2% of the low-power limit, and the photodiode sensitivity is almost zero. Increasing the reverse bias to 10 V increases the responsivity by only a factor of 3. The relative uncertainty of an energy measurement will exceed 100%. The reverse bias required in this case for reducing the uncertainty to 5% is 1.3 kV, well above the breakdown voltage of the photodiode. Clearly, the energy incident upon an EUVL wafer plane dosimeter must be significantly attenuated to enable the pulse energy to be measured with low uncertainty. This situation is exacerbated at the intermediate focus, where the average power is 30 times greater.

The reduction of both the integrated-charge and the peak-voltage responsivity with increasing pulse energy is due to the second calibration factor, β. This factor varies inversely with the geometric fill factor γ and thus varies directly with energy density $E_p/\gamma A$. For a given pulse energy, reducing the energy density by increasing the illuminated area of the photodiode should mitigate the effect of nonlinear responsivity on pulse-energy measurements. We do not expect the responsivity to vary significantly with pulse length in the proposed EUVL applications. Both the 10-ns pulse from a laser-produced plasma and the 200-ns pulse from a discharge source are much shorter than the photodiode discharge time, which is of the order of microseconds, and both sources essentially produce a delta-function optical pulse.

It is implicit in the discussion of integrated-charge responsivity that the lateral transport of majority carriers due to a diffusion current is negligible. The assumption is manifest in the equivalence of the majority carrier concentration and the energy density, as defined in Eq. (6). In fact, there will be a lateral transport current as majority carriers diffuse from the region of high concentration (the illuminated portion of the photodiode) to the region of low concentration. This diffusion will decrease the average energy density by causing the charge cloud to spread out. For a typical value[22] of the diffusion velocity of holes in Si (~50 m/s), the distance traveled by the majority carriers in the device's discharge time (~1 μs) is 50 μm, or 1% of the illuminated spot diameter. The average energy density is decreased by ~2%, as is the calibration value β_Q. For the photodiode studied here with 2-V reverse bias and 250-nJ incident pulse energy, this change in β_Q will raise the responsivity by only 0.4%, and the assumption of negligible effect from diffusion currents is validated.

These mechanisms for the reduction in responsivity make no reference to the fact that the sample detector is a Si p–n junction photodiode and should be relevant to all semiconductor photodiodes used to detect pulsed radiation. Richter *et al.* have measured[25] the linearity of a PtSi Schottky photodiode with a F_2 excimer laser at 157-nm wavelength and 10-ns pulse length. They observed that the peak-current signal is linear with ±4% uncertainty at

pulse energies below ~11 nJ and that the signal reaches a constant value at higher pulse energies. The response as a function of pulse energy is similar in form to the response shown in Fig. 6 of this paper. Their results with a PtSi Schottky photodiode are consistent with a nonlinear responsivity of the form described here. Additionally, wide-bandgap semiconductor photodiodes (SiC, AlGaN, etc.) in UV and IR detectors (InGaS, PbSe, etc.) should exhibit these effects. Although the various material properties will have different values, the predicted qualitative behavior is the same.

The authors are deeply indebted to many of our NIST colleagues: Keith Lykke for the cw calibration of the Si photodiode and helpful comments on the manuscript; Ping-Shine Shaw for the pyroelectric detector; Marla Dowell, Xiaoyu Li, and Holger Laabs for the pyroelectric detector calibration and discussions about the linearity of pyroelectric detectors; Charlie Tarrio and Simone Kulin for helpful discussions and comments on the manuscript; and Eva Wilcox for her work early on in this project. Ms. Wilcox was supported by the National Science Foundation through Research Experience for Undergraduates award 9605093. We are grateful to Bob Olsen of Scientech, Inc. for discussions about the proper use and limitations of pyroelectric detectors.

References

1. V. Banine, "Update on EUVL source requirements," presented at the Extreme Ultraviolet Lithography Source Workshop, Dallas, Tex., 14 October 2002.
2. C. Tarrio, R. E. Vest, and S. E. Grantham, "Absolute extreme-ultraviolet metrology," in *Harnessing Light: Optical Science and Metrology at NIST*, C. Londono, ed., Proc. SPIE **4450,** 94–107 (2001).
3. R. E. Vest, L. R. Canfield, M. L. Furst, R. M. Graves, A. Hamilton, L. R. Hughey, T. B. Lucatorto, and R. P. Madden, "NIST programs for radiometry in the far ultraviolet spectral region," in *Ultraviolet Atmospheric and Space Remote Sensing: Methods and Instrumentation II*, G. R. Carruthers and K. F. Dymond, eds., Proc. SPIE **3818,** 15–26 (1999).
4. R. Thornagel, R. Klein, and G. Ulm, "The electron storage ring BESSY II as a primary source standard from the visible to the x-ray range," Metrologia **38,** 385–389 (2001).
5. R. Stuik, F. Scholze, J. Tümmler, and F. Bijkerk, "Absolute calibration of a multilayer-based XUV diagnostic," Nucl. Instrum. Methods A **492,** 305–316 (2002).
6. J. F. Seely, C. N. Boyer, G. E. Holland, and J. L. Weaver, "X-ray absolute calibration of the time response of a silicon photodiode," Appl. Opt. **41,** 5209–5217 (2002).
7. R. Stuik and F. Bijkerk, "Linearity of p–n junction photodiodes under pulsed irradiation," Nucl. Instrum. Methods A **489,** 370–378 (2002).
8. D. E. Aspnes and A. A. Studna, "Dielectric functions and optical parameters of Si, Ge, GaP, GaAs, GaSb, InP, InAs, and InSb from 1.5 to 6.0 eV," Phys. Rev. B **27,** 985–1009 (1983).
9. R. Soufli and E. M. Gullikson, "Reflectance measurements on clean surfaces for the determination of optical constants of silicon in the extreme ultraviolet–soft-x-ray region," Appl. Opt. **36,** 5499–5507 (1997).
10. R. E. Vest, E. Wilcox, S. E. Grantham, and C. Tarrio, "Calibration of detectors for extreme ultraviolet lithography in pulsed radiation," presented at the NewRad Conference, Gaithersburg, Md., 20–24 May 2002.
11. R. Korde, J. S. Cable, and L. R. Canfield, "One gigarad passivating nitrided oxides for 100-percent internal quantum efficiency silicon photodiodes," IEEE Trans. Nucl. Sci. **40,** 1655–1659 (1993).
12. L. R. Canfield, "Photodiode detectors," in *Vacuum Ultraviolet Spectroscopy II*, J. A. R. Samson and D. L. Ederer, eds. (Academic, San Diego, Calif., 1998), pp. 117–138.
13. H. O. Funsten, D. M. Suszcynsky, S. M. Ritzau, and R. Korde, "Response of 100% internal quantum efficiency silicon photodiodes to 200 eV–40 keV electrons," IEEE Trans. Nucl. Sci. **44,** 2561–2565 (1997).
14. L. R. Canfield, J. Kerner, and R. Korde, "Stability and quantum efficiency performance of silicon photodiode detectors in the far ultraviolet," Appl. Opt. **28,** 3940–3943 (1989).
15. J. F. Seely, "Responsivity model for a silicon photodiode in the extreme ultraviolet," in *Instrumentation for UV/EUV Astronomy and Solar Missions*, S. Fineschi, C. M. Korendyke, O. H. W. Siegmund, and B. E. Woodgate, eds., Proc. SPIE **4139,** 1–7 (2000).
16. "NIST Optoelectronics Division Home Page," retrieved 19 December 2002, http://www.boulder.nist.gov/div815/.
17. H. Laabs and M. Dowell, Optoelectronics Division, National Institute of Standards and Technology, 325 Broadway, Boulder, Colo. 80305 (personal communication, 15 May 2002).
18. R. Korde, C. Prince, D. Cunningham, R. E. Vest, and E. Gullikson, "Present status of radiometric quality silicon photodiodes," Metrologia **40,** S145–S149 (2003).
19. S. W. Brown, G. P. Eppeldauer, and K. R. Lykke, "NIST facility for spectral irradiance and radiance responsivity calibrations with uniform sources," Metrologia **37,** 579–582 (2000).
20. "NIST Optical Technology Division Home Page," retrieved 19 December 2002, http://physics.nist.gov/Divisions/Div844/div844.html.
21. T. R. Gentile, J. M. Houston, and C. L. Cromer, "Realization of a scale of absolute spectral response using the National Institute of Standards and Technology high-accuracy cryogenic radiometer," Appl. Opt. **35,** 4392–4403 (1996).
22. B. Sapoval and C. Herman, *Physics of Semiconductors* (Springer-Verlag, New York, 1995).
23. P. Singh, "Lecture 11 from ECE 3590 Semiconductor Materials and Devices" (Villanova University, 11 June 1997), retrieved Nov 2002, http://www.ece.villanova.edu/~singh/lec11/sld027.html.
24. Technical Advisory Group 4, Metrology, *International Vocabulary of Basic and General Terms in Metrology*, 2nd ed. (International Organization for Standards, Geneva, Switzerland, 1993).
25. M. Richter, U. Kroth, A. Gottwald, C. Gerth, K. Tiedtke, T. Saito, I. Tassy, and K. Vogler, "Metrology of pulsed radiation for 157-nm lithography," Appl. Opt. **41,** 7167–7172 (2002).